Distance dependence of fluorescence enhancement from photonic crystal surfaces

Nikhil Ganesh, Patrick C. Mathias, Wei Zhang, and Brian T. Cunningham[a)]
Nano Sensors Group, Micro and Nanotechnology Laboratory, University of Illinois at Urbana-Champaign, 208 North Wright Street, Urbana, Illinois 61801, USA

(Received 21 January 2008; accepted 10 February 2008; published online 17 April 2008)

We experimentally verify the near-field nature of the fluorescence enhancement afforded by large area planar photonic crystal resonators. This is done by mapping the fluorescence enhancement factor for a fluorophore as a function of its distance above the device surface and comparing the results to numerical calculations. Experiments show that the decay of the enhancement factor is exponential as a function of distance from the device surface, and excellent agreement with the numerically calculated exponential decay length is obtained. In contrast to approaches involving surface plasmons on metal surfaces, we find that the maximum enhancement is obtained when the fluorophore is closest to the photonic crystal surface due to the absence of quenching at short distances. We also show that the decay length is largely controlled by the wavelength of light resonant in the device. © *2008 American Institute of Physics*. [DOI: 10.1063/1.2906175]

Enhancing the output of fluorescent species is highly desirable for a wide range of biological applications including DNA sequencing, gene expression, single molecule detection, and high resolution cell imaging. An extensive literature exists on the effects of metals on fluorophores and on the use of a variety of metal surface configurations (planar, corrugated, and islands) or metallic particle types (spheres, shells, boxes, and triangles, to name just a few) that involve plasmonic resonances to enhance fluorescence.[1] A relatively smaller variety of dielectric structures, such as waveguides and optical resonators, have been exploited for this purpose. Depending on distance and geometry, metal surfaces can cause increases in either quenching or enhancement of fluorescence.[2–5] The effects of metallic surfaces on fluorophores are due to at least three mechanisms: (1) energy transfer quenching to the metal via resonant energy transfer and, thus, lower fluorescent intensity, (2) increase in fluorescent intensity due to the metal amplifying the incident field, where the enhancement is due to the metal particles' ability to concentrate the excitation locally,[6,7] and (3) an increase in the intrinsic radiative decay rate of the fluorophore by providing an environment with enhanced photonic mode density,[8,9] resulting in Purcell enhancement.[10] With a wide variety of surface and structure configurations, plasmon-controlled fluorescence will have an important impact in many fields of biological science. However, surface plasmons present some inherent characteristics that are not ultimately the most desirable ones for enhanced fluorescence. First, quenching by the metal surface results in substantial loss of enhancement for any fluorophore within small distances from the surface—the same region where the metal enhanced near-fields have their greatest intensity. The quenching may be mitigated by the incorporation of spacer layers, at the cost of lowered enhancement factors. Second, the spectral width of surface plasmon resonances is generally large (~100 nm) due to the lossy nature of metals—essentially implying a resonance with a very low quality factor (Q factor). As an optical resonator, low Q factor results in relatively low stored electric field intensity, as energy is quickly dissipated in the metal. Recent reports show, for example, that in both electromagnetic computer simulations and actual experiments, the electric field amplitude at the resonant wavelength surrounding metal nanoparticles is ~2.5 times that of the incident electric field amplitude.[11]

Resonances occurring in periodic dielectric nanostructures have recently gained importance for a wide range of sensing, filtering, and feedback applications. Among such resonant structures, the guided-mode resonance (GMR) filter[12] based on one-dimensional and two-dimensional photonic crystal (PC) slabs has been the subject of intense study for the last two decades.[13–16] Although the far-field manifestation of the resonance (as a strong reflection peak whose central wavelength and line-width are arbitrarily tunable[17]) is well studied, only a few papers report on the near-field characteristics of such devices.[18,19] We have recently shown that due to the resonance occurring in PCs, the near-fields at an absorption wavelength of a fluorescent species can be greatly enhanced, and when this effect is combined with the coherent scattering phenomenon from the PC, PC enhanced fluorescence (PCEF) can be obtained.[20] In this paper, we theoretically and experimentally study the near-field characteristics of the fluorescence enhancement phenomenon. We determine the fluorescence enhancement factor as a function of the distance of the fluorophore from the resonator surface and qualitatively and quantitatively compare the results to predictions based on numerical calculations.

The GMR effect occurs when evanescent (cutoff) diffracted orders of a periodic subwavelength surface structure couple to the modes of an effective high index layer.[21] The energy is coupled to "leaky modes" which slowly radiate energy from the structure due to its diffractive nature, as waves that propagate in both the forward and backward di-

[a)]Electronic mail: bcunning@uiuc.edu.

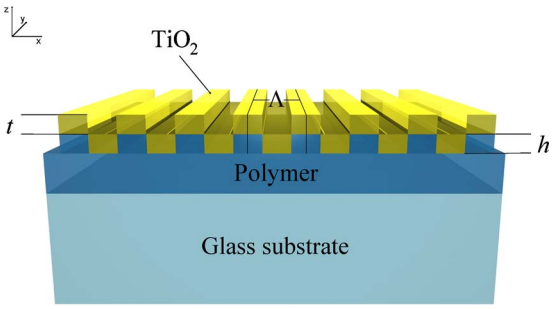

FIG. 1. (Color online) Layout of the one-dimensional photonic crystal slab displaying guided-mode resonances. The structure is comprised of a low refractive index polymer containing a one-dimensional periodic structure attached to a glass substrate and coated with a high index layer of TiO_2. The physical parameters of the device, refractive indices of the materials and the launch angle of the incident beam set the resonance wavelength

rections. These leaked out waves interfere with the directly transmitted and specularly reflected zeroth orders, leading to a strong reflection about a resonant wavelength whose linewidth and spectral location are set by the physical parameters of the device. The GMR effect leads to heightened energy density within the resonator under steady-state operation conditions (via continual reinforcement of the leaky modes by the externally incident illumination), the magnitude of which is directly related to the resonance Q factor, which, in turn, is inversely related to the resonance linewidth. A high resonance Q factor leads to high intensity near-fields with which fluorophores can interact and fluoresce with greater intensity, due to an enhanced absorption rate. GMRs with Q factors exceeding 2000 have been demonstrated in the past.[22]

The layout of the one-dimensional PC displaying GMRs and used in this study is shown in Fig. 1. The structure is comprised of a one-dimensional surface structure of height h, which is fabricated via a nanoreplica-molding process in a low refractive index (n) polymer. The structure is then coated with a layer of high n material of thickness t. The period of the surface structure is given by Λ. As a representative example, we study the response of such a device under external illumination using rigorous coupled-wave analysis[23] (RCWA). To fabricate the device, a high index titanium dioxide (TiO_2, $n_{TiO_2}=1.88$) film is coated upon a periodic surface structure in a polymer ($n_{poly}=1.46$). The period of the structure is $\Lambda=360$ nm (50% duty cycle) and the height of the surface structure is $h=100$ nm. The TiO_2 is coated to a thickness $t=160$ nm. To perform these simulations, a commercial implementation of two-dimensional RCWA was employed.[24] The index resolution and number of harmonics retained in the calculations as determined by convergence studies were ~1 nm and 30 harmonics, respectively. The materials were assumed to be lossless and dispersionless at about $\lambda=632.8$ nm. One period of the device was simulated with periodic boundary conditions applied in the x direction. The device is exposed to a superstrate, which in this study was assumed to be air.

When illuminated with white light, the device resonates for certain wavelengths that meet the phase-matching[25] condition. Due to different effective indices for the resonant modes depending on their polarization,[26] the resonant response is different depending on the polarization of the incidence. This is illustrated in the band structure calculations using RCWA simulations shown in Fig. 2, which shows the spectral location of the resonant reflection as a function of the launch angle (angle made with the normal to the device surface, in degrees) of a broadband source which is transverse electric (TE) [Fig. 2(a)] and transverse magnetic (TM) [Fig. 2(b)] polarized. The color scale shows the diffraction efficiency (far-field reflectivity). It is immediately evident that the device can be used to excite a broad range of resonant wavelengths by control of the launch angle and, therefore, the resonant wavelength can be made to overlap with the absorption wavelengths of a wide range of fluorophores. Also, it is seen that the TM resonances are narrower in linewidth, implying a higher Q-factor resonance for the same device structure. The calculated Q factors for the TE and TM modes for a wavelength $\lambda \sim 600$ nm are ~34 and ~370, respectively.

For the TE polarization, the incident electric field is polarized perpendicular to the plane of incidence, i.e., is comprised of an E_y electric field component and H_x/H_z magnetic field components (coordinate axis shown in Fig. 1). In the resonator steady state, E_y, H_x, and H_z components comprise of both resonant near-fields and propagating reflections. In

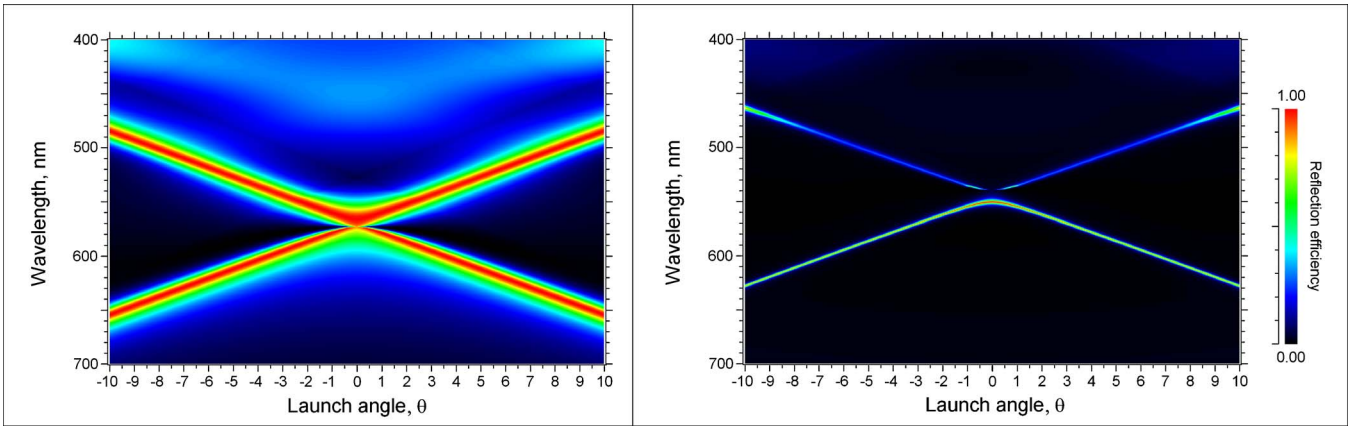

FIG. 2. (Color online) Calculated resonant mode band structure for the one-dimensional photonic crystal structure, shown for (a) TE polarized incidence and (b) TM polarized incidence. The y axis shows the spectral location of the resonance for a given incident angle in degrees (wave vector, x axis). The color scale shows the far-field reflectivity of the resonance, and the width of the bands are inversely related to the resonance Q factor.

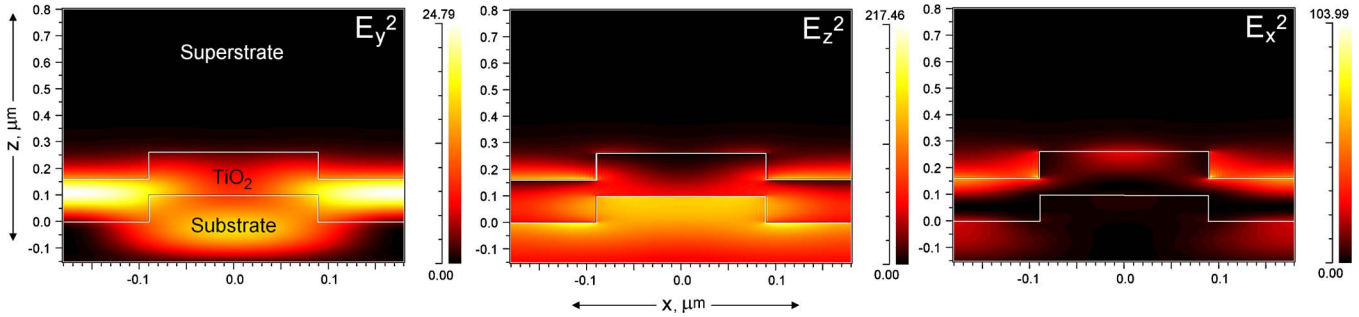

FIG. 3. (Color online) Calculated near-electric field intensity profiles for the resonant modes at $\lambda=632.8$ nm for (a) TE polarized incidence, showing enhancement of only the E_y field component and TM polarized incidence showing enhancement of both (b) E_z and (c) E_x field components. The color scale associated with each figure represents the intensity of the electric field and is normalized to the unit intensity incident wave.

contrast, the TM polarization is comprised of incident E_x/E_z electric field components and magnetic component H_y. The resonance causes E_x/E_z and H_y to define near-field components and propagating reflected waves, and the resonantly enhanced near fields. Since fluorescence processes mainly arise from electric dipole oscillations, only the electric-field components are considered in this work. The electric near fields produced by the device in response to both TE and TM polarized incidences are shown in Fig. 3. Figure 3(a) shows the electric field intensity (E_y^2) for TE polarized incidence. As is evident, the maximum near-field intensity occurs where the resonant mode is confined, with evanescent tails penetrating both the substrate and superstrate of the device. For the purpose of fluorescence enhancement, these enhanced fields represent a greater incident energy density. From the near-field plots in Figs. 3(b) and 3(c), we see the consequence of the higher Q-factor TM mode on the near-field intensity, which is clearly much greater than the TE case. Another point to note is that the TM resonance causes enhancement for both the E_x and E_z near-field components, which might be more beneficial (assuming similar overlap intensities for all the field components) than just the E_y field enhancement produced in the TE case, as the fluorophore dipole moments in ensemble experiments can be assumed to be equally distributed in all three dimensions. For the TM polarized case, the continuity of the displacement field across dielectric boundaries requires that the electric field must be lower in the higher index material, which is evident in Fig. 3(b) and 3(c). It is also understandable that the PCEF configuration is especially beneficial from the standpoint that the enhancement of fluorescence is maximally achieved for specifically bound fluorophores on the device surface and high signal-to-noise ratio is achievable, such as in the extremely sensitive total internal reflection fluorescence[27] configuration.

Having clarified the role of the resonance and the mechanism of the enhancement, we now consider the dependence of the enhancement factor as a function of the position of the fluorophore above the sensor surface. Characterizing the falloff of the fluorescence enhancement factor not only allows us to verify the near-field nature of the enhancement mechanism and to compare the operation of such devices with similar surface plasmon based devices but also enables us to determine the working range of such devices, to optimize the surface chemistry and ascertain limits on the physical sizes of the analytes that might be used. To study the distance dependence of fluorescence enhancement from these devices, we performed numerical simulations by using RCWA and compared the results to fluorescence experiments using an excitation wavelength of $\lambda=632.8$ nm. In the numerical calculations, various thicknesses of a silicon dioxide (SiO_2) spacer layer (which can be approximated as a biological material due to its low refractive index) were added to the device surface and then the average electric field intensity at the available surfaces was determined and plotted against the thickness of the SiO_2 layer. In these calculations, TE polarized light (the choice of this polarization was dictated by our measurement setup) was allowed to be incident on the device from below (along the $+z$ direction) and the launch angle was tuned to match the resonance at $\lambda=632.8$ nm for each thickness of SiO_2. The electric field intensity (E_y^2 field component for the TE polarization) at the top surface of the PC was averaged and plotted against the thickness of the SiO_2 spacer layer used in that simulation [Fig. 4(a)]. Size effects of the fluorophore and the surface chemistry were absent in these calculations. Theoretically, the field profile outside the device should be a simple exponential decay as is expected from the mode envelope of the confined wave; however, adding additional material to the device surface changes the effective index of the resonant mode and, consequently, its field distribution within the device. We observed that adding additional SiO_2 to the device caused the resonant mode profiles to be modified but not significantly affecting the decay of the field outside the device. The numerically calculated decay length (position at which the field is reduced to $1/e$ of its original value at the PC surface) as determined by fitting the electric field intensity (E_y^2) as a function of spacer layer thickness (for six values of the SiO_2 layer thickness as determined by experiment) to an exponential function was $d_{RCWA}=79.72$ nm. Experimentally, PC devices were fabricated by a process of nanoreplica molding[28] in a low index polymer by sandwiching the polymer between a prepatterned silicon master and a sheet of polyethylene terephthalate, curing the polymer, and peeling the structure off the master. To complete the devices, the required thicknesses of TiO_2 and SiO_2 were deposited by electron beam evaporation (Denton Vacuum). The thicknesses and the refractive indices of the dielectrics were measured by using spectroscopic ellipsometry (Woolam) and were used as inputs for the numerical calculations described above. The thicknesses of the SiO_2

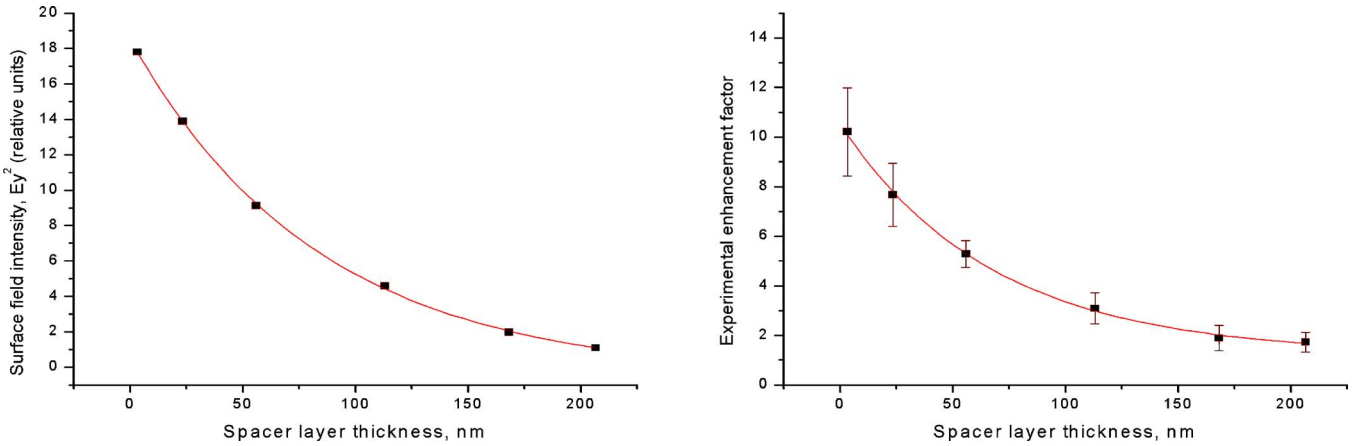

FIG. 4. (Color online) (a) Exponential decay of the electric field intensity on the surface of the device as a function of the thickness of the SiO_2 spacer, as calculated by RCWA. The decay length of the field intensity was $d_{RCWA}=79.72$ nm. (b) Experimentally determined falloff of the fluorescence enhancement factor for Cy-5 as a function of the thickness of SiO_2 layer deposited. The decay length determined by experiment was $d_{expt}=84.78$ nm. Both calculations and experiments were performed for an incident wavelength of $\lambda=632.8$ nm.

spacer layer ranged from $t_{SiO_2}=3.3$ to $t_{SiO_2}=206.6$ nm. The finished devices were subsequently mounted on microscope glass slides by using optical adhesive. To verify the distance dependence of the fluorescence enhancement, cyanine-5 (Cy-5) dye conjugated to streptavidin was immobilized on the surfaces of the devices (by spotting) and the fluorescence enhancement factor (ratio of fluorescence intensity from the dyes on and off resonance) was determined. To immobilize the dye attached to streptavidin, a 2% solution of aminopropyltriethoxy silane (Pierce) in acetone was applied to the SiO_2 terminated surface of the device, followed by 5 min incubation and washing procedure. Thereafter, incubation of the surface with 25% glutaraldehyde (Sigma Aldrich) was carried out for 2 h. This was followed by 15 h incubation with a 100 μg/ml solution of Cy-5 conjugated streptavidin (GE Healthcare), a subsequent wash with 0.05% Tween (Sigma Aldrich), and a 5 min ultrasonication in deionized water.

The prepared slides were scanned in a commercially available laser scanner (Tecan LS 2000, Tecan Ltd.) at a wavelength $\lambda=632.8$ nm. The scanner illuminates device with TE polarized incident light and a variable launch angle. The angle was controlled to match the resonance condition for each device to determine the enhanced fluorescence intensity and then changed to normal incidence to determine the nonresonant fluorescence intensity. Figure 4(b) shows the fluorescence enhancement factor plotted as a function of the SiO_2 layer thickness for each device. The experimentally obtained data were fitted to an exponential decay to obtain the average decay length, which was found to be $d_{expt}=84.78$ nm, in good agreement with the numerical calculations. It is also interesting to note that in comparison with similar enhancement schemes involving surface plasmon resonance, the effect of quenching of the fluorescence within some critical distance from the active surface is absent. As a representative example, Fig. 5 shows the case when the Cy-5 molecules are separated by a distance $t_{SiO_2}=3.3$ nm from the PC surface. The fluorescence scan on the left shows the fluorescence intensity for Cy-5 spots immobilized on the sensor surface under standard epifluorescence conditions (launch angle $\theta=0°$). The scan on the right shows the fluorescence intensity recorded when the launch angle is changed to match the $\lambda=632.8$ nm resonance ($\theta=6°$). As shown in the intensity scale below for a line scan, the average fluorescence enhancement for a modest Q factor and TE polarization is approximately ten times. It can also be appreciated that the fluorescence enhancement is uniformly seen over all the immobilized spots, over a large area and without any increase in the background signal.

We also studied the effect of the resonant wavelength on the fluorescence enhancement decay length. As evident from Fig. 2, resonances over a wide range of wavelengths can be excited by controlling the launch angle of the excitation. We calculated the decay lengths for excitation wavelengths ranging from $\lambda=488$ to 700 nm. The dispersion for the dielectrics was included in the simulation as the refractive index of the materials involved is expected to vary over this range. The results for this calculation are shown in Fig. 6. It is clearly seen that the normalized decay length (normalized to the decay length at $\lambda=640$ nm) strongly depends on the resonance wavelength. However, at lower wavelengths, the refractive index of TiO_2 begins to rapidly increase and causes stronger confinement of the resonant mode,[26] which results in the evident nonlinearity. In the region where the refractive indices of the material slowly vary, it is clear that the relationship between the decay length and the wavelength is linear as expected.[29] For the purpose of fluorescence based biosensing applications, this wavelength dependence of the enhancement decay rate can be utilized to accommodate the physical constraints of the application under consideration; for example, one might choose a fluorescent dye that absorbs at longer wavelengths when the sizes of the analytes are large, such as cells. For applications that require small volumes or demand a high degree of sensitivity toward material in close proximity to the surface of the sensor (e.g., DNA microarrays), lower wavelengths may be preferable as the shorter decay length will afford enhancement in a small range above the device surface.

In conclusion, we have demonstrated the near-field nature of the fluorescence enhancement mechanism using PC

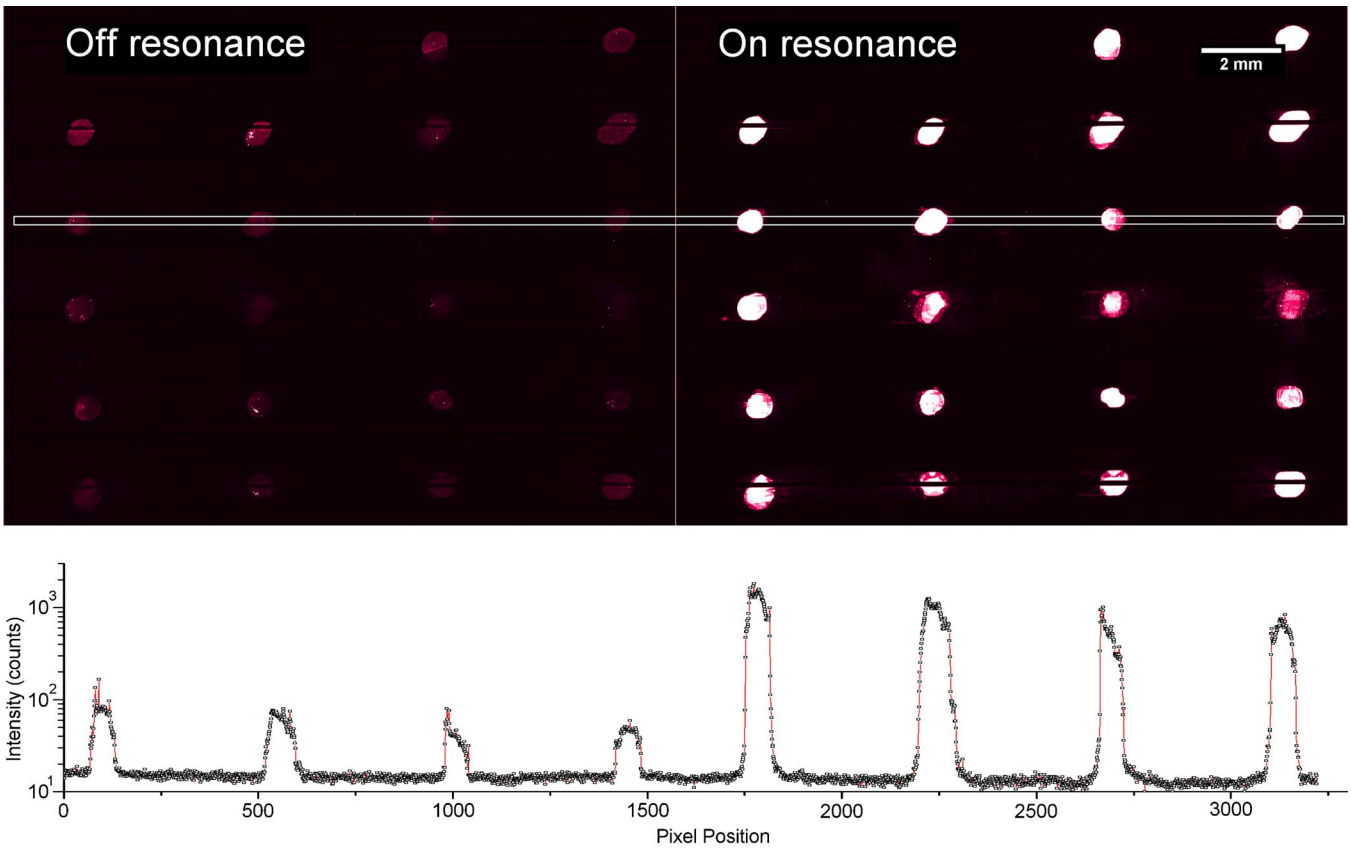

FIG. 5. (Color online) Fluorescence scans off (left) and on (right) resonance measured for a spacer layer thickness t_{SiO_2}=3.3 nm, showing the enhanced fluorescence effect. The plot below the figure shows the intensity profile on the sensor surface as a function of position, as marked by the line on the fluorescence scans.

slabs by experimentally verifying the exponential decay characteristics as predicted by numerical calculations. We also determined the average decay length of the fluorescence enhancement factor from the surface of the device, which for a resonant wavelength λ=632.8 nm, was found to be ~85 nm. We also showed that for a given set of material refractive indicies, the decay length is essentially controlled by the resonance wavelength.

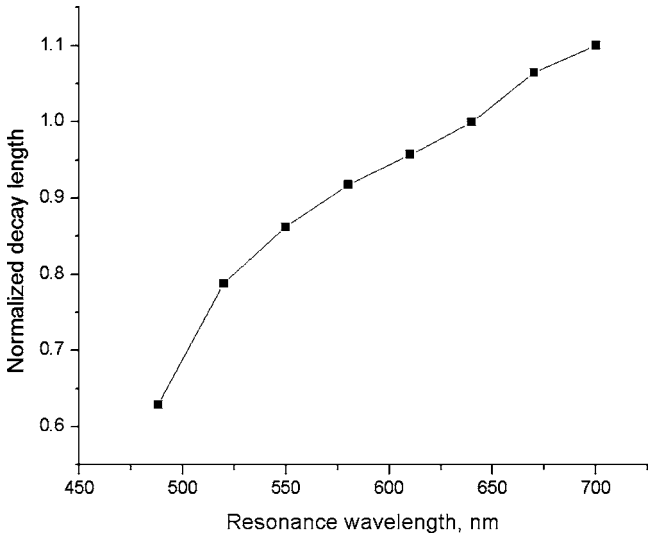

FIG. 6. Variation of the decay length with the resonance wavelength: Calculated decay lengths (normalized to the decay length at λ=640 nm) as a function of the resonant wavelength. The relationship is approximately linear in the wavelength range where the dispersion of the materials is small. Toward lower wavelengths, the increasing index of the materials causes greater confinement of the resonant mode resulting in the observed nonlinearity.

This work was supported by the National Science Foundation under Grant No. 0427657. Any opinions, findings, and conclusions or recommendations expressed in this material are those of the author(s) and do not necessarily reflect the views of the National Science Foundation. The authors gratefully acknowledge SRU Biosystems for providing financial support for this work. The authors also extend their gratitude to the support staff of the Micro and Nanotechnology Laboratory at the University of Illinois at Urbana-Champaign.

[1]J. R. Lakowicz, Plasmonics **1**, 5 (2006).
[2]A. M. Glass, P. F. Liao, J. G. Bergman, and D. H. Olson, Opt. Lett. **5**, 368 (1980).
[3]A. Campion, A. R. Gallo, C. B. Harris, H. J. Robota, and P. M. Whitmore, Chem. Phys. Lett. **73**, 447 (1980).
[4]K. Sokolov, G. Chumanov, and T. N. Cotton, Anal. Chem. **70**, 3898 (1998).
[5]K. L. Kelly, E. Coronado, L. L. Zhao, and G. C. Schatz, J. Phys. Chem. B **107**, 668 (2003).
[6]T. Hayakawa, S. T. Selvan, and M. Nogami, Appl. Phys. Lett. **74**, 1513 (1999).
[7]S. T. Selvan, T. Hayakawa, and M. Nogami, J. Phys. Chem. B **103**, 7064 (1999).
[8]J. R. Lakowicz, Anal. Biochem. **298**, 1 (2001).
[9]W. L. Barnes, J. Mod. Opt. **45**, 661 (1998).
[10]E. M. Purcell, Phys. Rev. **69**, 681 (1946).
[11]J. Zhang, Y. Fu, M. H. Chowdhury, and J. R. Lakowicz, Nano Lett. **7**,

2101 (2007).
[12]R. Magnusson and S. S. Wang, Appl. Phys. Lett. **61**, 1022 (1992).
[13]H. L. Bertoni, L. H. S. Cheo, and T. Tamir, IEEE Trans. Antennas Propag. **37**, 78 (1989).
[14]V. N. Astratov, I. S. Culshaw, R. M. Stevenson, D. M. Wittaker, M. S. Skolnick, T. K. Krauss, and R. M. D. L. Rue, J. Lightwave Technol. **17**, 2050 (1999); S. Boonruang, A. Greenwell, and M. G. Moharam, Appl. Opt. **45**, 5740 (2006).
[15]A. Rosenberg, M. Carter, J. Casey, M. Kim, R. Holm, R. Henry, C. Eddy, V. Shamamian, K. Bussmann, S. Shi, and D. Prather, Opt. Express **13**, 6564 (2005).
[16]S. Peng and G. Michael Morris, Opt. Lett. **21**, 549 (1996).
[17]S. S. Wang and R. Magnusson, Appl. Opt. **32**, 2606 (1993).
[18]Y. Ding and R. Magnusson, Opt. Express **12**, 1885 (2004).
[19]C. Wei, S. Liu, D. Deng, J. Shen, J. Shao, and Z. Fan, Opt. Lett. **31**, 1223 (2006).
[20]N. Ganesh, W. Zhang, P. C. Mathias, E. Chow, J. A, N. T. Soares, V. Malyarchuk, A. D. Smith, and B. T. Cunningham, Nat. Nanotechnol. **2**, 515 (2007).
[21]D. Rosenblatt, A. Sharon, and A. A. Friesem, IEEE J. Quantum Electron. **33**, 2038 (1997).
[22]A. S. P. Chang, S. Bai, H. Tan, W. Wu, Z. Yu, and S. Y. Chou, Proceedings of the LEOS 2002, Glasgow, Scotland, 2002 (unpublished).
[23]M. G. Moharam and T. K. Gaylord, J. Opt. Soc. Am. **71**, 811 (1981).
[24]RSOFT DIFFRACTMOD.
[25]R. Magnusson, Y. Ding, K. J. Lee, D. Shin, P. S. Priambodo, P. P. Young, and T. A. Maldonado, Proc. SPIE **5225**, 20 (2003).
[26]I. D. Block, N. Ganesh, M. Lu, and B. T. Cunningham, IEEE Sens. J. **8**, 274 (2008).
[27]L. Tamm, *Optical Microscopy: Emerging Methods and Applications*. (Academic, New York, 1993).
[28]N. Ganesh and B. T. Cunningham, Appl. Phys. Lett. **88**, 071110 (2006).
[29]N. Ganesh, I. D. Block, and B. T. Cunningham, Appl. Phys. Lett. **89**, 023901 (2006).